Strong electron-electron interactions of a Tomonaga-Luttinger liquid observed in InAs quantum wires

Yosuke Sato,[1,*,†] Sadashige Matsuo,[1,2,3,*,‡] Chen-Hsuan Hsu,[3] Peter Stano,[1,3,4] Kento Ueda,[1] Yuusuke Takeshige,[1] Hiroshi Kamata,[3] Joon Sue Lee,[5] Borzoyeh Shojaei,[5,6] Kaushini Wickramasinghe,[7] Javad Shabani,[7] Chris Palmstrøm,[5,6,8] Yasuhiro Tokura,[9] Daniel Loss,[3,10] and Seigo Tarucha[1,3,§]

[1]Department of Applied Physics, University of Tokyo,7-3-1 Hongo, Bunkyo-ku, Tokyo 113-8656, Japan
[2]JST, PRESTO, 4-1-8 Honcho, Kawaguchi, Saitama 332-0012, Japan
[3]Center for Emergent Matter Science, RIKEN, 2-1 Hirosawa, Wako-shi, Saitama 351-0198, Japan
[4]Institute of Physics, Slovak Academy of Sciences, 845 11 Bratislava, Slovakia
[5]California NanoSystems Institute, University of California Santa Barbara, Santa Barbara, California 93106, USA
[6]Materials Engineering, University of California Santa Barbara, Santa Barbara, California 93106, USA
[7]Center for Quantum Phenomena, Department of Physics, New York University, New York, New York 10003, USA
[8]Electrical and Computer Engineering, University of California Santa Barbara, Santa Barbara, California 93106, USA
[9]Faculty of Pure and Applied Sciences, University of Tsukuba, Tsukuba, Ibaraki 305-8571, Japan
[10]Department of Physics, University of Basel, Klingelbergstrasse 82, CH-4056 Basel, Switzerland

(Received 29 October 2018; revised manuscript received 5 March 2019; published 16 April 2019)

We report strong electron-electron interactions in quantum wires etched from an InAs quantum well, a material generally expected to have strong spin-orbit interactions. We find that the current through the wires as a function of the bias voltage and temperature follows the universal scaling behavior of a Tomonaga-Luttinger liquid. Using a universal scaling formula, we extract the interaction parameter and find strong electron-electron interactions, increasing as the wires become more depleted. We establish theoretically that the spin-orbit interaction cause only minor modifications of the interaction parameter in this regime, indicating that genuinely strong electron-electron interactions are indeed achieved in the device. Our results suggest that etched InAs wires provide a platform with both strong electron-electron interactions and the strong spin-orbit interaction.

DOI: 10.1103/PhysRevB.99.155304

I. INTRODUCTION

A one-dimensional electron system displays the physics of a Tomonaga-Luttinger liquid (TLL), which is strikingly different to Fermi liquids in higher dimensions. A spinful TLL is described by the Hamiltonian [1,2]

$$H = \sum_{\nu=\mathrm{c,s}} \int \frac{\hbar dx}{2\pi} \left\{ u_\nu g_\nu [\partial_x \theta_\nu(x)]^2 + \frac{u_\nu}{g_\nu} [\partial_x \phi_\nu(x)]^2 \right\}. \quad (1)$$

Here, $\nu \in \{\mathrm{c,s}\}$ labels the charge and spin sector, respectively, while u_ν are the velocities, and θ_ν and ϕ_ν the bosonic fields, describing the two elementary excitations [3]. The electron-electron (e-e) interactions are parameterized by g_c and g_s, which range between 0 and 1 [4]. The spin-charge separation, meaning the independence of the charge and spin sectors displayed by Eq. (1), appears as one of the key features of a TLL.

The coupling of spin and charge degrees of freedom, in various forms of the spin-orbit interaction (SOI), plays an important role in semiconductors and spintronics [5,6]. The research on SOI has been further accelerated by predictions of the emergence of Majorana fermions in an accessible setup comprising a quantum wire with superconductivity, SOI, and a magnetic field [7–10]. Unfortunately, the practical realization is impeded by the incompatibility of a strong magnetic field and superconductivity. Recently, it has been suggested that wires with strong e-e interactions could solve this conflict by disposing of the magnetic field [11,12]. More importantly, strong e-e interactions allow a realization of parafermions [11], more advanced topological particles than the Majorana fermions [13,14]. They rely on Cooper pair splitting into two quantum wires with high efficiency, which is achieved through strong e-e interactions. We note that efficient Cooper pair splitting [15,16] and a transparent interface with a superconductor has been recently demonstrated in self-assembled InAs nanowires [17,18] and quantum wells [19]. With this outlook, providing wires with both strong e-e interactions and strong SOI seems beneficial.

Motivated by such prospects, there appeared several theoretical works concerned with a TLL in the presence of SOI. The SOI mixes the spin and charge sectors and a rich range of phenomena was predicted, from mild modifications to a breakdown of the TLL phase [20–32]. Despite active discussions in theory, there are only few experimental studies of TLL physics in wires with strong SOI. Concerning InAs, we note the self-assembled nanowires [33] and nanowire

*These authors contributed equally to this work.
†yosuke.sato0530@gmail.com
‡sadashige.matsuo@riken.jp
§tarucha@riken.jp

 ©2019 American Physical Society

quantum point contacts [34] experiments. In the former, a small interaction parameter was deduced, but it remained unclear whether this was due to the SOI, intrinsically strong e-e interactions, or even some other physics. The situation contrasts to TLLs without SOI, with a number of reports, for example on GaAs wires [35–38], carbon nanotubes [39–44], all in which the SOI is negligible. Overall the effects of SOI in TLLs have been considered in theory but have been explored in few experimental studies.

II. SUMMARY OF THE MAIN RESULTS

Here we investigate the TLL behavior of quantum wires fabricated in an InAs quantum well. Even though we do not quantify its strength in this experiment, it is generally expected that the SOI in InAs is strong [45–47]. We measure the electric current through the wires as a function of the bias voltage at various temperatures and find that the data falls onto a single curve upon rescaling. Such universal scaling is consistent with the TLL theory, allowing extraction of the value of the interaction parameter g_c in Eq. (1). The extracted values reach as low as 0.16–0.28 (these minimal values are for wires close to depletion), indicating a strong-interaction regime. In addition to transport measurements, we provide theoretical understanding of one-dimensional systems with strong e-e interactions and SOI. Overall our results demonstrate that InAs wires offer a platform fulfilling the requirements for the realization of topological particles.

III. DEVICE

The data presented in this paper were measured on a single device,[1] shown in Fig. 1(a). It is composed of ten parallel quantum wires, which were chemically etched from an InAs quantum well. Ohmic contacts, created using Ti/Au [48], and a Ti/Au top gate, deposited on top of a cross-linked PMMA serving as an insulating layer, give electrical access and control. A single wire has a length of 20 μm and a nominal width (estimated from the depth of the etching) of 100 nm. The stack materials of the InAs quantum well are given in Fig. 1(b). Prior to measurements of the wires, the two-dimensional electron gas mobility of 7.2×10^4 cm/(Vs), electron density of 3.4×10^{11} cm^{-2}, and mean free path of 690 nm were extracted from measurements on a Hall-bar device at 560 mK. The electric current I flowing through the parallel wires upon applying a bias voltage V is measured by the standard four-terminal dc measurement. These measurements are performed at temperature T in the range 2–4 K. Figure 1(c) shows I as a function of the top gate voltage V_g for a fixed $V = 1$ mV. The device shows a pinch-off at about $V_g = -0.86$ V. A small current remaining below that voltage is most probably due to a tunneling conductance through quantum dots formed in the disorder potential of the wires. The parallel quantum wire structure reduces the total resistance such that the total current is still within the measurable range. Though measuring many parallel wires precludes observing conductance plateaus, it also results in averaging out the potential fluctuations from impurities and other disorder. We believe that such averaging is crucial for observing the universal scaling we report.

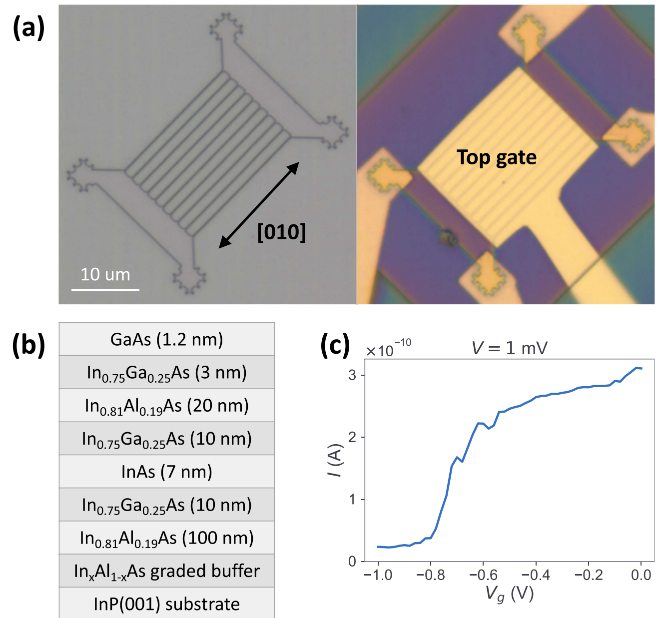

FIG. 1. (a) Microscope photographs of the parallel-wire device before (left) and after (right) depositing a top gate above a cross-linked PMMA layer. The wires are along [010]. (b) Schematic structure of the wafer, grown along [001]. (c) Gate voltage dependence of the current through the wires measured at a constant source-drain voltage as given in the figure caption. This measurement is performed at 2.9 K.

IV. UNIVERSAL SCALING OF THE CURRENT-VOLTAGE CURVE

Before presenting our main results, we first review the transport properties predicted by the existing theory. It has been established that, *assuming the spin-charge separation*, a current through a single TLL with several tunnel barriers (their number and positions are discussed below) displays universal scaling [39,49]. Explicitly, the tunnel current is

$$I = I_0 T^{1+\alpha} \sinh\left(\frac{\gamma e V}{2k_B T}\right)\left|\Gamma\left(1+\frac{\alpha}{2}+\frac{i\gamma e V}{2\pi k_B T}\right)\right|^2. \quad (2)$$

Here, I_0 is an unspecified overall scale dependent on a typical barrier strength, $\Gamma(z)$ is the Gamma function, e is the positive elementary charge, k_B is the Boltzmann constant, and the parameters α and γ depend on the number and character of the barriers, or, more generally, source of resistance.[2]

[1] We fabricated several devices with various lengths and numbers of wires in search for characteristic features of TLL. These early devices were plagued by typically large contact resistances and a wafer-dependent voltage range of the few-channel regime. The next generation of devices will build on this experience.

[2] Below, we consider the current-voltage relation (alternatively, the conductance) under more general conditions than that under which Eq. (2) has been originally derived. In such general considerations, we use the name "sources of resistance" without specifying whether

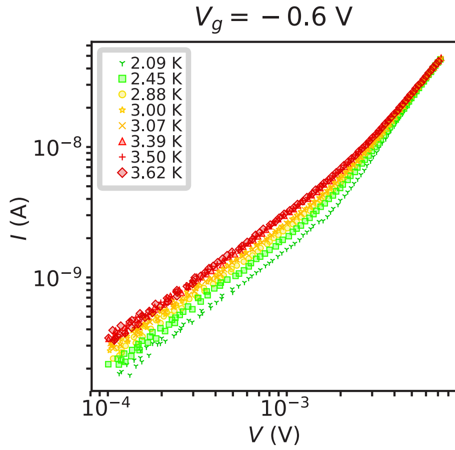

FIG. 2. Current (I) flowing through the wires as a function of the bias voltage (V) for the top gate voltage $V_g = -0.6$ V.

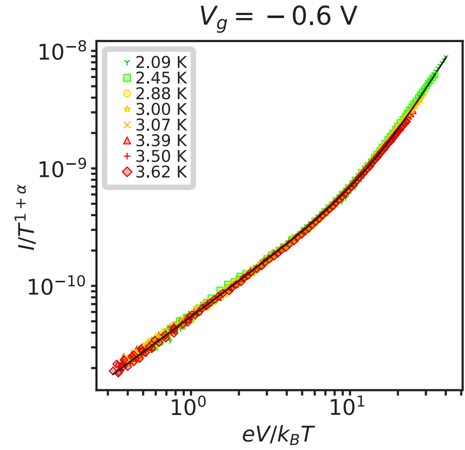

FIG. 3. A rescaled current $I/T^{1+\alpha}$ as a function of eV/k_BT from the data points in Fig. 2. The black-solid curve is drawn using Eq. (2) with the parameters $(\alpha, \gamma, I_0) = (1.3,\ 0.38,\ 3.6\times^{-10}\mathrm{A/K}^{2.3})$, which were extracted by fitting the data in Fig. 2 to Eq. (2). We note that the unit of I_0 scales with α.

The expression γV corresponds to a voltage drop across the tunnel barrier. Thus, in Ref. [49], one has $\gamma = 1$. One can generalize this result to several, say N, tunnel barriers; assuming that they induce comparable resistances, a typical voltage drop over a single one will be V/N. For this case,[3] the inverse of γ therefore gives the number of tunnel barriers [39,50].

The parameter α depends in an intricate way on the e-e interaction strength parameters g_c and g_s, the SOI strength, and the number and character of the sources of resistance. The expressions for α for the case of zero SOI are already known. For the case of finite SOI, we provide them here and in Ref. [51]. Extracting this parameter from the data and inferring from it the e-e interaction strength is the essence of this paper. Let us first describe the former task, before discussing the latter one.

The extraction of α is rather straightforward once the I-V curve in Eq. (2) is plotted on a log-log scale. This exercise reveals different slopes for γeV much smaller and much larger than k_BT. For the (differential) conductance, $G \equiv dI/dV$, this corresponds to power laws $G \propto T^\alpha$ and $G \propto V^\alpha$, respectively. The power law in the conductance, $G \propto T^\alpha$, in the regime of $eV \ll k_BT$, was observed in numerous previous experiments [38–43,50,52–57]. If the universal scaling curve is obtained for a large enough range of its natural parameter, eV/k_BT, such that the crossover is seen, one can extract both γ and α.

V. MEASUREMENT OF *I-V* CURVES AND FIT TO EQ. (2)

To extract both α and γ, we measure the current I as a function of the bias voltage V at various temperatures. A set of such curves, for top-gate voltage of $V_g = -0.6$ V, is shown in Fig. 2. One can see that the current generally decreases with decreasing temperature T, and that for a fixed T different slopes for the high-V and low-V regimes can be observed. These features are qualitatively consistent with Eq. (2). For a fixed top-gate voltage V_g, we fit the whole set of I-V curves to Eq. (2) with I_0, α, and γ as the fitting parameters. The rescaled data, together with the fitted curve, is plotted in Fig. 3. We observe that the rescaled data indeed collapses onto a single curve, confirming the universal scaling behavior of a TLL.

After confirming that the universal scaling holds, and therefore the parameters α and γ are reasonably assigned by the fit, we examine their dependence on the carrier density. As the latter is tunable through the top gate voltage, we repeat the above measurements and fittings for various V_g, and summarize the results in Fig. 4 (Fig. 7 in Appendix A 3 shows three more sets, for $V_g = -0.2$, -0.4, and -0.8 V, with both raw and scaled I-V data from which the fittings are performed). One can see that both parameters change with V_g, suggesting

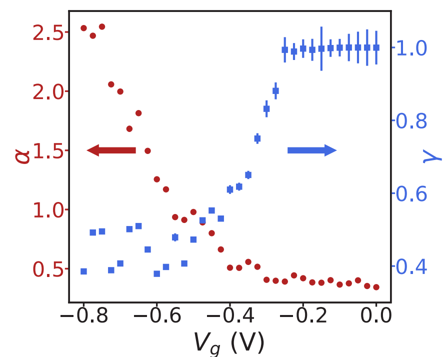

FIG. 4. Fitted values of α as a function of the top gate voltage V_g (red circle, left axis). The error bars of the fitting are smaller than the markers. Fitted values of γ as a function of V_g are also plotted (blue squares, right axis). For $V_g > -0.25$ V, the fitted values of γ are not very reliable, as reflected by the larger error bars.

tunnel barriers, weak impurities or other scatterers. We argue that Eq. (2) is still valid in this more general situation, upon proper interpretation of parameters I_0, α, and γ.

[3]We stress that the connection between γ and the number of barriers N is $\gamma = 1/N$ only if all the barriers result in identical resistances. Otherwise, γ counts only the barriers which dominate the voltage drop. The typical (length) density of these dominating barriers might have no direct relation to the transport mean free path found for the 2DEG, as will be the case here.

that the e-e interaction strength varies with the carrier density. To convert the extracted parameters to physical parameters of the system is rather involved and will be addressed later. Before that, we consider the observation of the fitted values of γ collapsing to 1 for voltages $V_g > -0.25\,\mathrm{V}$. As we already stated, the fitted value of γ is determined by the position of the kink in the current-bias curve (for example, in Fig. 3, the kink is at $eV/k_{\mathrm{B}}T \approx 10$). However, the smaller the value of α the smaller the variation in gradient between low- and high-V regimes, complicating the determination of the kink position. Our fits are less sensitive to γ for $\alpha \lesssim 0.5$, where the fit returns $\gamma = 1$. Though error bars become larger, the value $\gamma = 1$ is consistent with the trend observed where γ is accurately extracted for higher α. Nevertheless, the most interesting part of this plot is on its left end, for large negative values of the top gate V_g. Here, α is large which corresponds to strong e-e interactions, as we will see. Also, in the same region, γ is around 0.5, corresponding to two tunnel barriers. We are primarily interested in extracting the strength of the e-e interactions in this regime.

VI. DEDUCING THE STRENGTH OF ELECTRON-ELECTRON INTERACTIONS

A. Description of the theoretical methods used

We now describe our theoretical analysis, which allows us to extract the strength of the e-e interactions from the observed α. Motivated by the expected strong SOI in InAs, we model each of the wires as a TLL subject to SOI. To this end, we incorporate the SOI-induced band distortion, which is parametrized by the ratio $\delta v/v_F$ with δv the velocity difference between the two branches of the distorted energy bands [58] (see Appendix B for details). This band distortion breaks the spin-charge separation of a TLL in Eq. (1) [20,21] and leads to a coupling between the charge and spin sectors [see Eq. (B1) in Appendix B]. In addition, the SOI can cause the value of g_s to depart from unity [22,30]. In deriving the current-voltage characteristics, we include both the charge-spin coupling in the Hamiltonian and a general value for the g_s parameter.

The theoretical analysis is complicated not only by the presence of the SOI, but also by the fact that the conductance depends on the characters and positions of the resistance sources (strong or weak, and inside the wire or around its boundary) and also on the value of α itself (larger or smaller than 0.5). Including these features is what sets our work apart from preceding studies. For the sake of brevity, we delegate the full analysis to Ref. [51] and state the main results from there in Appendix B. Here, in the main text, we distill that results further, and only give and comment on the formulas which are used to fit the experimental data.

We start with that, first, we observe γ roughly between 1 and 1/2, and, second, that we expect disorder to be generally present in the wires.[4] Correspondingly, we begin with considering the following types of resistance sources: a single tunnel barrier located in the wire bulk, a single tunnel barrier located near the wire boundary, and a disorder potential from many weak impurities. We first calculate the corresponding resistances separately, and then discuss the total wire resistance when they coexist.

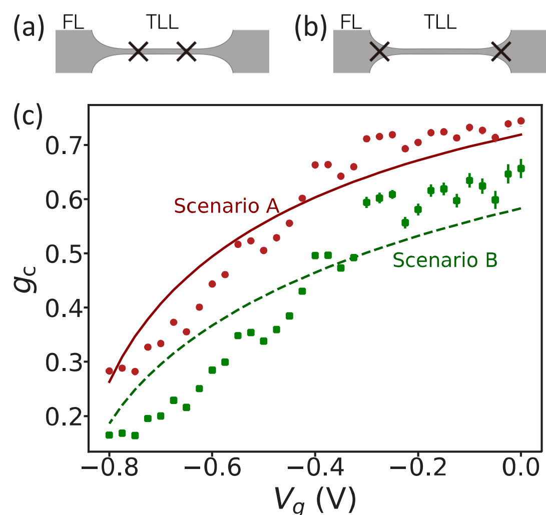

FIG. 5. (a) A schematic illustration of scenario A: there are bulk barriers (crosses), each acting as a TLL-TLL junction, and many weak impurities (not shown). (b) A schematic illustration of scenario B: there are boundary barriers, each acting as a TLL-Fermi liquid (FL) junction, and many weak impurities. In (a) and (b), for illustration, we plot two barriers, motivated by the observed $1/\gamma \lesssim 2$. (c) Extracted values of the interaction parameter g_c as a function of the top gate voltage V_g for the two scenarios. The red-solid and green-dashed curves are the fits to Eq. (6), with the fitting parameter w (the wire transverse size) being 87 and 47 nm, respectively.

In the presence of a single bulk or boundary barrier, we compute the tunnel current through it using the method of Ref. [49], which allows one to obtain the full current-bias curve. In addition, we use the renormalization-group (RG) method of Refs. [59,60] to obtain the current power-law scaling in the high-temperature and high-bias limits. We verify that, in these limits, the two theoretical approaches give the same exponent α and are therefore consistent.

For many weak impurities (that is, disorder potential), the method of Ref. [49] is not applicable. Instead, we calculate the exponent of the current power law in the high-temperature and high-bias limits using the RG method of Refs. [59,60]. In this case, we understand Eq. (2) as an interpolation formula, with the parameter α replaced by the computed exponent of the power law and with $\gamma = 1$ regardless of the number of weak impurities.

With the above results, we consider the situation with coexisting tunnel barriers and weak impurities. There are following possible scenarios: (A) all barriers are in the wire bulk, being TLL-TLL junctions, as illustrated in Fig. 5(a), (B) all barriers are near the wire boundaries, being junctions between a TLL and a Fermi-liquid lead; see Fig. 5(b), (C) There are both bulk and boundary tunnel barriers. In each case, in addition to the barriers, the disorder potential is also present. Fortunately, as in the data we observe γ close to 1/2 or larger, we can restrict out treatment to considering up to

[4]As the wires are much longer than the bulk mean free path of 690 nm, the disorder (perhaps, in the form of weak potential modulation due to impurities) should play role in the wire resistance.

two barriers in total. This assumption reduces scenario C to a single case, with one bulk and one boundary barrier. We can then exclude this case, as it would give different scaling behavior in the high-bias and high-temperature regimes [50], in contrast to what we observe.

Left with only scenarios A and B, the single barrier resistance can be directly generalized to multiple barriers of comparable strengths by replacing $V \to \gamma V$. To estimate the total wire resistance, we assume that the contributions from tunnel barriers and weak disorder are additive. To treat them in the same way, we use the RG method to determine the power law of the current-voltage dependence for both. Due to the distinct power laws for these sources, we can identify a single term which dominates the resistance (in the RG sense) for a given strength of e-e interactions. In each scenario, keeping only the dominant term, we conclude that the current-voltage relation is described by Eq. (2), and obtain the expressions for α in terms of the intrinsic interaction parameters g_c and g_s, and the ratio $\delta v/v_F$, as given below.

Finally, in order to convert the observed power α to the value of g_c, we need the values of the SOI-induced parameters, $\delta v/v_F$, and the departure of g_s from 1. For parameters relevant to our experiment, we estimate $\delta v/v_F \lesssim 0.1$. As $1-g_s$ scales with the same quantity, $\delta v/v_F$ [30], we find that the modification in g_s is similarly small [22]. Our quantitative analysis presented in Appendix B 1 concludes that such small values have negligible influence on the relation between α and g_c, meaning that to interpret the data of our device, we can use the zero-SOI expressions for α.[5] In addition, when the wires are close to being depleted, which is the strong-interaction regime of our primary interest, $\delta v/v_F$ becomes vanishingly small, making our approximations even more accurate. We note that, even with these approximations, the conversion from the observed α to g_c is still complicated due to various types of resistance sources. In the following, we present the derived expression of α and its approximated form for scenarios A and B. We use the approximate form to extract the value of g_c from the value of α observed.

B. Conversion of α to g_c in scenario A (bulk tunnel barriers and weak disorder)

In scenario A, the tunnel current is given by Eq. (2) with α given by (see Appendix B)

$$\alpha_{\text{bulk}} = \left(\frac{1}{g'_c} + \frac{1}{g'_s}\right)\left(\cos^2\theta + g_0^2 \sin^2\theta\right) - 2 \tag{3a}$$

$$\approx \frac{1}{g_c} - 1, \tag{3b}$$

where the approximation is valid for parameters relevant here. In the above, θ is a small parameter characterizing the strength of the SOI, and the explicit forms of g'_ν, g_0, and θ are given in Appendix B. On the other hand, the interpolation formula for weak impurities is given by Eq. (2), with $\gamma = 1$ and α being

$$\alpha_{\text{imp}} = 2 - \cos^2\theta(g'_c + g'_s) - g_0^2 \sin^2\theta\left(\frac{1}{g'_c} + \frac{1}{g'_s}\right), \tag{4a}$$

$$\approx 1 - g_c, \tag{4b}$$

where the second line again stems from the approximation valid for our parameters. Importantly, for any repulsive interaction $g_c \leqslant 1$, the approximated value is bounded $\alpha_{\text{imp}} \leqslant 1$, allowing us to rule out the weak impurities as the source of the observed value $\alpha > 1$ in the low-V_g regime. Further, for any $g_c < 1$, one has $1/g_c - 1 > 1 - g_c$, such that the resistance from the bulk tunnel barriers dominates that from weak impurities. We therefore assign the observed power law to bulk barriers and use

$$\alpha_A = \frac{1}{g_c} - 1, \tag{5}$$

to extract the g_c values from the data in Fig. 4. In Fig. 5(c), we plot the extracted g_c as a function of V_g. The lowest value $g_c = 0.28$ corresponds to very strong e-e interactions in a wire with low electron density.

To further check the consistency of our procedure, we fit the extracted g_c to the formula [59,61]

$$g_c = \left[1 + \frac{e^2}{\pi^2 \varepsilon \hbar v_F} \ln\left(\frac{D^2}{dw}\right)\right]^{-1/2}. \tag{6}$$

In this equation, derived by estimating the compressibility of the electron gas with the Coulomb interaction screened by a conducting plane (the top gate), D is the distance between the wire and the top gate, d is the quantum well thickness, w is the wire width, and ε is the dielectric constant. For our device, we have $D = 300$ nm, $d = 7$ nm, and $\varepsilon = 15.15\,\varepsilon_0$ [62]. Using w as a fitting parameter, we get the red curve in Fig. 5(c), showing a good correspondence with g_c fitted from the data. Further, the fitted value $w = 87$ nm is consistent with the nominal width of 100 nm. Given w, we estimate the wire subbands level spacing $\frac{\hbar^2}{2m^*}(\frac{2\pi}{w})^2 \approx 8.64$ meV corresponding to E_F at $V_g = -0.54$ V.[6] This estimate suggests that our device is in the single-channel regime for $V_g < -0.54$ V, where an approximately constant value of $\gamma \simeq 1/2$ is seen in Fig. 4.[7] Given all these cross-checks, we conclude that scenario A provides a consistent interpretation of the measured data.

[5] This conclusion also means that, even though the TLL is spin-orbit coupled, the strength of the SOI cannot easily be extracted from the quantities that we measure; for that purpose, different quantities or experiments would have to be pursued.

[6] From the stacking structure of the wafer, we estimate the Fermi energy $E_F = 1.13 \times 10^2 \times [V_g - (-0.86)]^2$ (meV) and the Fermi velocity $v_F = 1.31 \times 10^{13} \times [V_g - (-0.86)]w$ (m/s) (see Appendix A 2). Here, V_g is in units of V, w is in units of m.

[7] The level spacing is large enough that we can ignore higher subbands at the temperatures of our measurements. In Ref. [77], the subband level spacing in a 100-nm-diameter InAs nanowire with isotropic cross-section as found to be approximately 8 meV, which is similar to our estimate here.

TABLE I. Deduced interaction parameters (g_c) of one-dimensional systems as reported in experiments, including the present work (shaded row). The description of the entries is as follows. The first column gives the material(s) used in the listed references. The second column lists the extracted α parameter (if available) from the observed quantity given in the sixth column. Based on the resistance sources attributed in the references, the corresponding parameters $\alpha_{\rm bulk}$, $\alpha_{\rm end}$ and $\alpha_{\rm imp}$ are given (we label those with unspecified sources with an unsubscripted α). The third and fourth columns list the interaction parameter g_c either quoted from the references (in black) or deduced from the α value (in red) using Table II below. The third column includes the g_c value deduced from $\alpha_{\rm bulk}$ or those with unknown sources. The fourth column includes those from either $\alpha_{\rm end}$ or $\alpha_{\rm imp}$. For α value with unknown resistance sources, we deduce g_c values for all impurity types considered here. The extracted γ value (if available) is given in the fifth column. The notations G, T, and R denote the conductance, temperature, and resistance, respectively. The abbreviations NW, CNT, VG, and CE stand for nanowire, carbon nanotube, V groove, and cleaved edge, respectively.

Material [Ref]	Extracted α from experiment	g_c deduced[a] from $\alpha_{\rm bulk}$	g_c deduced[b] from $\alpha_{\rm end}$ or $\alpha_{\rm imp}$	γ	Observed quantity
MoSe NW [50]	$\alpha_{\rm bulk}=0.61$–6.6; $\alpha_{\rm end}=0.94$–5.2	0.13–0.62	0.09–0.35 ($\alpha_{\rm end}$)	0.25[c]	$G\propto T^{\alpha}$
InAs NW	$\alpha=0.35$–2.5	0.28–0.74	0.16–0.65 (both)	0.5–1.0	Eq. (2)
Multiwall CNT [41]	$\alpha_{\rm end}=0.36$–0.95	–	0.21–0.41 ($\alpha_{\rm end}$)	0.05–0.24	G[d]
InAs NW[e] [33]	–	0.23[f]	–	–	$G_{\rm max}\propto T^{\frac{1}{g}-2}$[g]
Single-wall CNT [40]	$\alpha_{\rm bulk}=1.4$	0.26	–	0.6[c]	$G\propto T^{\alpha}$
Multiwall CNT [42]	$\alpha_{\rm bulk}=1.24$; $\alpha_{\rm end}=0.6$[h]	0.29	0.29 ($\alpha_{\rm end}$)	–	$G\propto T^{\alpha}$
Single-wall CNT [39]	$\alpha_{\rm end}=0.6$[h]	–	0.29 ($\alpha_{\rm end}$)	0.46–0.63[c]	$G\propto T^{\alpha}$
$NbSe_3$ NW [53]	$\alpha_{\rm bulk}=2.15$–2.2	0.31–0.32	–	$\frac{1}{100}$–$\frac{1}{77}$[c]	$R\propto T^{-\alpha}$
GaAs VG [37]	–	–	0.45–0.66 ($\alpha_{\rm imp}$)	–	δG_1[i]
GaAs/AlGaAs CE [63]	$\alpha_{\rm imp}=0.5$	–	0.50 ($\alpha_{\rm imp}$)	–	δG_1
GaAs VG [38]	–	0.54–0.66	–	–	$G\propto T^{\frac{1}{g_c}-1}$
Single-wall CNT [44]	–	0.55	–	–	STM imaging
GaAs/AlGaAs [36]	–	0.6	–	–	$\Delta R_{\rm bs}$[j]
GaAs/AlGaAs [35]	–	–	0.65–0.7 ($\alpha_{\rm imp}$)	–	δG_1
GaAs/AlGaAs CE [64]	–	0.66–0.82	–	–	$\Gamma_i\propto T^{\frac{1}{g_c}-1}$[k]
GaAs NW[l] [43]	$\alpha=0.02$–0.23	0.81–0.98	0.77–0.98 ($\alpha_{\rm imp}$)[m]	–	$G\propto T^{\alpha}$
Multiwall CNT [55]	$\alpha=0.02$–0.05	0.91–0.96	0.90–0.96 ($\alpha_{\rm imp}$)[n]	–	$G\propto T^{\alpha}$

[a]Here we use $\alpha_{\rm bulk}=1/g_c-1$ for NWs and $\alpha_{\rm bulk}=(1/g_c-1)/2$ for CNTs. Note that here we intentionally use the same notation g_c for both NWs and CNTs; see Table II for general expressions.
[b]Here we use $\alpha_{\rm end}=(1/g_c-1)/2$ and $\alpha_{\rm imp}=1-g_c$ for NWs, and $\alpha_{\rm end}=(1/g_c-1)/4$ and $\alpha_{\rm imp}=(1-g_c)/2$ for CNTs; see Table II for details.
[c]In this reference, while the universal scaling behavior was observed and thus the γ value was obtained, the value for α was extracted from the power-law conductance rather than from the full current-voltage curve.
[d]On top of the universal scaling conductance, additional phenomenological parameters are required for their fitting.
[e]In this reference, the device forms a quantum dot.
[f]This reference reported a small value 0.38 for the effective interaction parameter $g=(1/2g_c+1/2g_s)^{-1}$, which was attributed to $g_s<1$ due to the SOI. In contrast, our work indicates that the effects of the SOI on the interaction parameter are negligible for relevant strength of the SOI. With the assumption $g_s=1$, the value of g_c in this reference becomes 0.23. We use the latter value for the table entry here.
[g]The notation $G_{\rm max}$ denotes the conductance value of the Coulomb peak.
[h]In this reference, the tunnel conductance from a FL lead into *the bulk of a TLL* is also measured. It leads to a different power law, whose exponent is, however, not discussed in our work.
[i]The notation δG_1 denotes the conductance correction of the first conductance plateau.
[j]The notation $\Delta R_{\rm bs}$ denotes the backscattering resistance due to Bragg reflection.
[k]The notation Γ_i denotes the full width at half maximum of a Coulomb peak.
[l]In this reference, a core-shell nanowire was used.
[m]Alternatively, assuming that disorder is absent within the wire, the g_c value deduced from $\alpha_{\rm end}$ follows as 0.68–0.96.
[n]Alternatively, assuming that disorder is absent within the nanotube, the g_c value deduced from $\alpha_{\rm end}$ follows as 0.83–0.93.

C. Conversion of α to g_c in scenario B (boundary tunnel barriers and weak disorder)

We now consider scenario B, in which the tunnel current through the boundary barriers is given by Eq. (2) with (see Appendix B)

$$\alpha_{\rm end}=\frac{1}{2}\left(\frac{1}{g_c'}+\frac{1}{g_s'}\right)\left(\cos^2\theta+g_0^2\sin^2\theta\right)-1 \tag{7a}$$

$$\approx\frac{1}{2g_c}-\frac{1}{2}. \tag{7b}$$

The contribution of weak impurities is the same as in scenario A, characterized by $\gamma=1$ and $\alpha_{\rm imp}\approx 1-g_c$. In contrast to scenario A, weak impurities now become dominant over boundary tunnel barriers for $\alpha<0.5$. The observed parameter α is therefore related to the interaction parameter g_c through

$$\alpha_{\rm B}\approx\begin{cases}\frac{1}{2g_c}-\frac{1}{2}, & \text{for } \alpha\geqslant 0.5 \text{ (barriers);}\\ 1-g_c, & \text{for } \alpha\leqslant 0.5 \text{ (impurities).}\end{cases} \tag{8}$$

The extracted g_c is shown in Fig. 5(c) along with the fit to Eq. (6). Here, the g_c values are even smaller than in scenario A and reach as low as 0.16.

Next, we discuss how additional features of the extracted values for α and γ fit with the assumptions of scenario B. Namely, as V_g decreases the extracted γ value decreases from unity and approaches 0.5 around $V_g = -0.4$ V. At the same voltage, α steps across 0.5, which is the transition point between the two expressions in Eq. (8). Such a feature can be well captured by scenario B, where γ should be unity when weak impurities dominate and 1/2 when the boundary tunnel barriers dominate. The fit to Eq. (6) gives a value $w =$ 47 nm and the associated subband level spacing of 29.6 meV, indicating that the wire is in the single-channel regime for $V_g < -0.23$ V, where the extracted γ drops below 1. Thus we conclude that scenario B is also in agreement with several aspects of the data.

D. Conclusion on the considered scenarios

Both scenarios A and B are reasonable and capture salient features of the experimental data such that it is difficult to exclude one or the other. Scenario A gives somewhat better agreement with Eq. (6); however, we do not deem a quantitative discrepancy to such a simple theory as very informative. Arguably, the weak point of scenario A is the observation that each wire contains two tunnel barriers in its interior.[8] On the contrary, in scenario B, the tunnel barriers are formed near the wire ends and having two per wire is more natural. Nevertheless, we emphasize that regardless of which scenario is realized, both support our main conclusion that strong and gate-tunable e-e interactions are present in the wires.

VII. COMPARISON TO E-E INTERACTION STRENGTHS REPORTED IN LITERATURE

Before concluding, we compare the e-e interaction strength found here with previous experiments. To make sensible comparison of numerous references, we convert—whenever possible—to unified parameters, being g_c and α in the notation of this paper. We include one-dimensional systems regardless of materials or measurement types and arrive at Table I, with entries ordered by the lowest value of g_c achieved in a given reference. In general, systems with well-defined single channels (e.g., single-wall carbon nanotubes) tend to have smaller values of g_c (stronger interactions[9]) due to suppression of scattering and stronger spatial confinement. A smaller mass of InAs compared to GaAs is also beneficial for a smaller g_c, giving a larger level spacing and a well-defined single channel.

VIII. CONCLUSIONS

To conclude, we investigate quantum wires etched from an InAs quantum well and find that they possess strong e-e interactions. This finding is based on observation of universal scaling of the current as a function of the bias voltage and temperature, from which the TLL interaction parameter can be fitted. The fitting requires a theory for the conversion of the observed exponent α of the power-law dependence of the conductance to the e-e interaction strength parameter g_c in the TLL Hamiltonian. The relation between α and g_c depends on the character and positions of the sources of resistance. For the case of finite SOI, we provide the main results of such theory here. Its most important conclusion is that for strong e-e interactions, the effects of the SOI on the relation between α and g_c are negligible. This reassures us that the large values of α that we observe are due to genuinely strong e-e interactions, and not, for example, an artifact of strong SOI. All together, our work demonstrates that an etched InAs quantum wire is a promising platform offering a quasi one-dimensional channel with strong and gate-tunable e-e interactions.

ACKNOWLEDGMENTS

This work was partially supported by a Grant-in-Aid for Young Scientific Research (A) (Grant No. JP15H05407), a Grant-in-Aid for Scientific Research (B) (Grant No. JP18H01813), a Grant-in-Aid for Scientific Research (A) (Grant No. JP16H02204), a Grant-in-Aid for Scientific Research (S) (Grant No. JP26220710), Japan Society for the Promotion of Science Research Fellowship for Young Scientists (Grant No. JP18J14172), Grants-in-Aid for Scientific Research on Innovative Area "Nano Spin Conversion Science' (Grants No. JP17H05177), a Grant-in-Aid for Scientific Research on Innovative Area "Topological Materials Science" (Grant No. JP16H00984) from MEXT, Japan Science and Technology Agency CREST(Grant No. JPMJCR15N2), JST PRESTO (Grant No. JPMJPR18L8), the ImPACT Program of Council for Science, and Technology and Innovation (Cabinet Office, Government of Japan). H.K. acknowledges support from RIKEN Incentive Research Projects and JSPS Early-Career Scientists (Grant No. JP18K13486). Y.T. acknowledges support from Japan Society for the Promotion of Science through Program for Leading Graduate Schools (MERIT). The authors would like to thank Michihisa Yamamoto and Ivan V. Borzenets for support of experiment and measurement equipment, and Russell S. Deacon for proofreading.

---

[8] If they originate in random disorder, there is no reason for such uniformity. On the other hand, one could argue that disorder averaged over many parallel wires might result in a scaling curve with some effective number of tunnel barriers, being here close to 2. However, performing such type of fitting would require the adoption of some *ad hoc* assumptions about the statistical distributions of the strength and position of the tunnel barriers. We, therefore, do not follow this method of analysis.

[9] In the TLL model that we work with here, the constants g are the only parameters defining the strength of the electron-electron interactions. The value of the Fermi velocity, indicating the relation of the kinetic to interaction energies, would also need to be considered to judge the "strength" of the interactions in a broader context. Here, we do not consider such implications and when we discuss the e-e interaction strength we are solely making statements on the value of constants g.

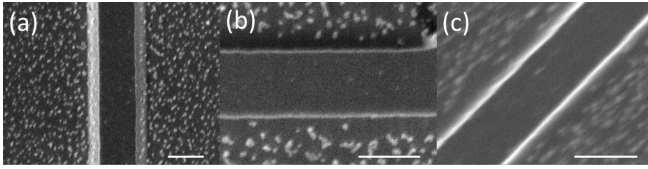

FIG. 6. SEM images of quantum wires chemically etched out from the wafer grown along [001] direction. The wires are along (a) $[1\bar{1}0]$, (b) [110], and (c) [010] direction, respectively. The scale bar in each figure indicates the length of 500 nm. From the brightness of the edges compared to dots surrounding the wires, each wire's cross-section is inferred as a trapezium, a reverse trapezium and a rectangle, respectively.

APPENDIX A: EXPERIMENTAL DETAILS

1. Chemical etching and crystal axis

To form our Hall-bar and quantum-wire devices, we use chemical etching by diluted H_2O_2 and H_2SO_4. It is well known that the rates of etching speed depend on the crystal axis of the samples, consequently so do the edge shapes of the devices. We tested the etching process on a trial wafer and confirmed such dependency by SEM. Figure 6 shows SEM images of wires formed in (a) $[1\bar{1}0]$, (b) [110], and (c) [010] direction. The SEM image reflects the slope of edges, and therefore it enables us to identify cross-sections of these wires as a trapezium, a reverse trapezium and a rectangle, respectively. Based on these findings, we choose to measure on wires formed along [010] direction so that we can determine the width of the quantum wires more precisely, being the same as the width of their top-surface.

2. Estimation of the gate dependence of electronic density in wires

From the stacking structure of the quantum well and 260-nm-thick cross-linked polymethyl methacrylate (PMMA), we estimate the top gate capacitance of 2.71×10^{-16} F. We take the dielectric constants of PMMA and InAlAs to be 4 and 13.59, respectively [65,66]. With this we estimate the Fermi energy $E_\mathrm{F} = 1.13 \times 10^2 \times [V_g - (-0.86)]^2$ (meV) and the carrier density $n = 8.31 \times 10^5 \times [V_g - (-0.86)]$ (cm^{-1}), respectively. Owing to the high mobility of the quantum well, longer uniform quantum wires can be realized compared to self-assembled nanowires [33].

3. Current-bias data for various V_g

Here, we show additional plots of current as a function of bias voltage, for various V_g (Fig. 7). All the sets of raw data in Figs. 7(a)–7(c) show good universal scaling, as evidenced in Figs. 7(d)–7(f).

FIG. 7. Current as a function of bias voltage with various V_g. The first row is the raw data and the second is fitted and scaled data. We evaluate $(\alpha, \gamma, I_0) = (0.42,\ 1.0,\ 2.9 \times 10^{-9}\ \mathrm{A/K^{1.42}})$, $(0.51,\ 0.61,\ 2.2 \times 10^{-9}\ \mathrm{A/K^{1.51}})$, and $(2.5,\ 0.38,\ 7.7 \times 10{-}13\ \mathrm{A/K^{3.5}})$ for $V_g = -0.2, -0.4$ and -0.8 V, respectively.

APPENDIX B: THEORETICAL ANALYSIS

In this Appendix, we present the main results of our theoretical analysis. We first discuss the effects of the spin-orbit interaction (SOI). We then provide formulas which we use to extract the interaction parameters in various scenarios. In addition, we summarize the expressions of the exponent α for various Tomonaga–Luttinger liquid (TLL) systems in existing literature.

1. Effects of SOI

In this section, we discuss the effects of SOI on the power-law conductance and current-voltage curve of a TLL. The motivation for this calculation is to examine how the SOI affects the observed parameter α. Namely, whereas the observed universal scaling behavior in the current-voltage characteristics unambiguously establishes the TLL behavior of our quantum wires, it remains to be clarified whether the rather large α value (implying small g_c) in the low-density regime is not an illusion owing to the expected strong SOI in InAs.

First of all, we remark that it is known that in the absence of a magnetic field, the SOI can be gauged away in strictly one-dimensional system, thereby having no influence on observable quantities [30,67,68]. In a quasi-one-dimensional geometry such as the etched quantum wires in our experiment, however, the interplay between the SOI and the transverse confinement potential that defines a finite width of the quantum wire can modify the band structure, leading to different velocities for different branches in the spectrum [58,68]. It was shown that such an effect destroys the spin-charge separation [20,21], leading to a coupling between the spin and charge sectors in Eq. (1) in the main text.

To investigate whether such a coupling alters the observed α value, we theoretically analyze its effects on the current-voltage characteristics. In the following, we first outline our calculation based on the TLL formalism, and then give our results on various types of resistance sources. To be specific, we consider impurities which are either strong or weak (acting as tunnel barriers or potential disorder), and for the former type we further consider whether they locate in the bulk or at the boundaries (ends) of the wires.

Before continuing, let us comment on possible origins of the tunnel barriers at the boundaries of the wire. We first clarify that these "boundary barriers" may be located close to, but not exactly at the physical boundary between the wire and a lead. As discussed in Ref. [49], a barrier can be considered a boundary one if its distance from the wire boundary is shorter than the scales $\hbar v_F/(k_B T)$ and $\hbar v_F/(eV)$. Since for our experiments these length scales are typically of order $O(100\text{ nm})$–$O(1\,\mu\text{m})$, observing boundary tunnel barriers is plausible.

To proceed, we follow Refs. [20,21] and add the following term to Eq. (1) of the main text:

$$H_{\rm so} = \delta v \int \frac{\hbar dx}{2\pi} \{[\partial_x \phi_{\rm c}(x)][\partial_x \theta_{\rm s}(x)] + [\partial_x \phi_{\rm s}(x)][\partial_x \theta_{\rm c}(x)]\}. \tag{B1}$$

It reflects the presence of SOI as a velocity difference δv between the two branches of the energy spectrum. Since the full Hamiltonian $H + H_{\rm so}$ is still quadratic in the bosonic fields, we can diagonalize it to get

$$H' \equiv H + H_{\rm so} = \sum_{\nu=c,s} \int \frac{\hbar dx}{2\pi} \left\{ u'_\nu g'_\nu [\partial_r \theta'_\nu(x)]^2 + \frac{u'_\nu}{g'_\nu} [\partial_x \phi'_\nu(x)]^2 \right\}, \tag{B2a}$$

where the modified TLL parameters and velocities are given by

$$g'_{\rm c} = \frac{g_{\rm c} g_0}{g_{\rm s}} \left[\frac{(g_0^2 + g_{\rm s}^2) + (g_{\rm s}^2 - g_0^2)\cos(2\theta) + g_0 g_{\rm s}^2 \frac{\delta v}{v_F} \sin(2\theta)}{(g_0^2 + g_{\rm c}^2) + (g_0^2 - g_{\rm c}^2)\cos(2\theta) + g_0 g_{\rm c}^2 \frac{\delta v}{v_F} \sin(2\theta)} \right]^{1/2}, \tag{B2b}$$

$$g'_{\rm s} = \frac{g_{\rm s} g_0}{g_{\rm c}} \left[\frac{(g_0^2 + g_{\rm c}^2) + (g_{\rm c}^2 - g_0^2)\cos(2\theta) - g_0 g_{\rm c}^2 \frac{\delta v}{v_F} \sin(2\theta)}{(g_0^2 + g_{\rm s}^2) + (g_0^2 - g_{\rm s}^2)\cos(2\theta) - g_0 g_{\rm s}^2 \frac{\delta v}{v_F} \sin(2\theta)} \right]^{1/2}, \tag{B2c}$$

$$u'_{\rm c} = \frac{v_F}{2 g_0 g_{\rm c} g_{\rm s}} \left[(g_0^2 + g_{\rm c}^2) + (g_0^2 - g_{\rm c}^2)\cos(2\theta) + g_0 g_{\rm c}^2 \frac{\delta v}{v_F} \sin(2\theta) \right]^{1/2} \times \left[(g_0^2 + g_{\rm s}^2) + (g_{\rm s}^2 - g_0^2)\cos(2\theta) + g_0 g_{\rm s}^2 \frac{\delta v}{v_F} \sin(2\theta) \right]^{1/2}, \tag{B2d}$$

$$u'_{\rm s} = \frac{v_F}{2 g_0 g_{\rm c} g_{\rm s}} \left[(g_0^2 + g_{\rm s}^2) + (g_0^2 - g_{\rm s}^2)\cos(2\theta) - g_0 g_{\rm s}^2 \frac{\delta v}{v_F} \sin(2\theta) \right]^{1/2} \times \left[(g_0^2 + g_{\rm c}^2) + (g_{\rm c}^2 - g_0^2)\cos(2\theta) - g_0 g_{\rm c}^2 \frac{\delta v}{v_F} \sin(2\theta) \right]^{1/2}, \tag{B2e}$$

with the parameters

$$g_0 = \frac{\sqrt{2} g_{\rm c} g_{\rm s}}{\sqrt{g_{\rm c}^2 + g_{\rm s}^2}}, \tag{B2f}$$

$$\theta = \frac{1}{2} \arctan\left(\frac{\delta v}{v_F} \frac{\sqrt{2} g_{\rm c} g_{\rm s} \sqrt{g_{\rm c}^2 + g_{\rm s}^2}}{g_{\rm s}^2 - g_{\rm c}^2} \right). \tag{B2g}$$

In the absence of the SOI, we have $(\delta v, \theta) \to (0, 0)$, and therefore $(g'_c, g'_s, u'_c, u'_s) \to (g_c, g_s, u_c, u_s)$. Using the model in Ref. [58], we have estimated that for the parameters relevant to our experiments, the value of $\delta v/v_F$ is at most around 0.1 and becomes vanishingly small when the system is close to being depleted. We remark that Ref. [20] obtains a similar estimate, of $\delta v/v_F \approx 0.1$–0.2.

With the diagonalized Hamiltonian Eq. (B2a), we are able to compute the tunnel current and the conductance of the quantum wires. Leaving the details for a separate publication [51], here we state our results and discuss their relevance to our experiment.

As mentioned in the main text, we consider several scenarios in which different types of resistance are present. We first consider a single tunnel barrier in the bulk, modeled as a TLL-TLL junction, and compute the current through it. For relevant strength of SOI, we obtain Eq. (2) in the main text, with the parameters $\gamma = 1$ and α replaced by

$$\alpha_{\text{bulk}}(g'_c, g'_s, \theta) = \left(\frac{1}{g'_c} + \frac{1}{g'_s}\right)\left(\cos^2\theta + g_0^2 \sin^2\theta\right) - 2, \tag{B3}$$

where the arguments (g'_c, g'_s, θ) are themselves functions of $(g_c, g_s, \delta v)$. The exponent Eq. (B3) is given in Eq. (3) in the main text. In the presence of several bulk barriers with comparable resistances, the tunnel current through the wire is given by Eq. (2) with the same α_{bulk} as Eq. (B3) and with γ equal to the inverse of the barrier number.

An alternative approach based on the renormalization-group tools [59,60] can be employed to compute the power-law conductance in the high-temperature ($k_B T \gg eV$) and high-bias ($eV \gg k_B T$) limits. In the presence of a single bulk barrier, the power-law conductance can be summarized as

$$G_{\text{bulk}}(T, V) \propto \text{Max}(k_B T, eV)^{\alpha_{\text{bulk}}}, \tag{B4}$$

which is characterized by the same parameter α_{bulk}. Similar to the tunnel current, the above formula can be generalized for several bulk barriers upon replacing $V \to \gamma V$ with $1/\gamma$ being the barrier number. It can be shown that $G_{\text{bulk}}(T, V)$ is consistent with the current-voltage characteristics [Eq. (2) in the main text] in the high-temperature and high-bias limits, demonstrating the compatibility of the two approaches.

We now analyze how the SOI influences the current-voltage characteristics through the parameter α_{bulk}. It is useful to define an effective interaction parameter $g_{c,\text{eff}}$, such that all the effects of $\delta v/v_F$ are incorporated into a single parameter. To be specific, we define $g_{c,\text{eff}}^{\text{bulk}}$ by the following relation:

$$\alpha_{\text{bulk}}(g'_c, g'_s, \theta) \equiv \alpha_{\text{bulk}}\left(g_{c,\text{eff}}^{\text{bulk}}, 1, 0\right) = \frac{1}{g_{c,\text{eff}}^{\text{bulk}}} - 1. \tag{B5}$$

This leads to the following definition for $g_{c,\text{eff}}^{\text{bulk}}$,

$$\frac{1}{g_{c,\text{eff}}^{\text{bulk}}} \equiv \left(\frac{1}{g'_c} + \frac{1}{g'_s}\right)\left(\cos^2\theta + g_0^2 \sin^2\theta\right) - 1, \tag{B6}$$

which describes the relation between the apparent interaction parameter $g_{c,\text{eff}}$ (corresponding to the extracted g_c from our experimental observation) and the intrinsic parameters g_c, g_s, and δv. We remark that the exponent of the power-law conductance does not depend on the number of barriers, so the definition of $g_{c,\text{eff}}$ is the same for single and multiple barriers in the wire.

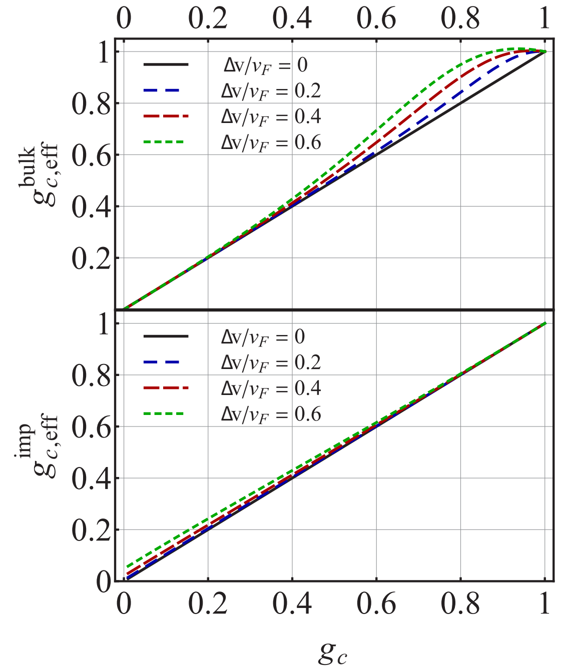

FIG. 8. Effective interaction parameter $g_{c,\text{eff}}$ as a function of the actual interaction parameter g_c for various values of the ratio $\delta v/v_F$. (Top) In the case of tunnel barriers, $g_{c,\text{eff}}^{\text{bulk}}$ is defined in Eq. (B6). (Bottom) In the case of weak impurities, $g_{c,\text{eff}}^{\text{imp}}$ is defined in Eq. (B9).

To visualize the effects of the SOI on $g_{c,\text{eff}}^{\text{bulk}}$, we plot it as a function of g_c for several values of $\delta v/v_F$, as displayed in the top panel of Fig. 8. Note that we intentionally include exaggerated values of $\delta v/v_F \geqslant 0.2$ in the plot; a more realistic value $\delta v/v_F \lesssim 0.1$ leads to barely visible changes. Further, while rather strong SOI does modify the parameter $g_{c,\text{eff}}^{\text{bulk}}$, we find two important features relevant to our experiments. First, $g_{c,\text{eff}}^{\text{bulk}}$ increases with an increasing strength of SOI. Therefore, the SOI cannot make the apparent interaction constant $g_{c,\text{eff}}^{\text{bulk}}$ smaller than g_c. Second, the SOI-induced increase of $g_{c,\text{eff}}^{\text{bulk}}$ is sizable in the weak- or moderate-interaction regime ($0.5 \leqslant g_c \leqslant 1$), but becomes negligible for the strong-interaction regime ($g_c \leqslant 0.5$). Thus, these features allow us to neglect the SOI when extracting the value of g_c in the case of bulk barriers. We emphasize that such an approximation is more accurate (becoming practically exact) in the low-V_g (small g_c) regime, which is our primary interest.

We now move on to the case of a tunnel barrier located around a boundary of the wire, which acts as a TLL-Fermi liquid (FL) junction. Again, we compute the tunnel current for generic temperatures and bias voltages, as well as the power-law conductance $G_{\text{end}} \propto \text{Max}(k_B T, eV)^{\alpha_{\text{end}}}$ in the high-temperature and high-bias limits. In this case, the tunnel current and the power-law conductance are the same as those for a bulk barrier, except that the exponent reads

$$\alpha_{\text{end}} = \left(\frac{1}{2g'_c} + \frac{1}{2g'_s}\right)\left(\cos^2\theta + g_0^2 \sin^2\theta\right) - 1, \tag{B7}$$

from which we can define the same parameter $g_{\mathrm{c,eff}}$ as in Eq. (B6). Again, in the presence of several barriers, we have the same exponent α_{end} and $V \to \gamma V$. Similar to α_{bulk}, a realistic value of the ratio $\delta v/v_F$ cause only a minor modification of the α_{end} values, justifying our procedure on the extraction of the g_{c} value using the zero-SOI formula [Eq. (7b) in the main text].

We now turn to the case of weak impurities, modeled as a backscattering potential. In this case, the calculation for a tunnel barrier in Ref. [49] is not applicable. We therefore compute the conductance using the method of Refs. [59,60]. The corresponding exponent in the high-temperature and high-bias limits is

$$G_{\mathrm{imp}}(T,V) \propto \mathrm{Max}(k_BT, eV)^{\alpha_{\mathrm{imp}}}, \tag{B8a}$$

$$\alpha_{\mathrm{imp}} = 2 - \cos^2\theta(g_{\mathrm{c}}' + g_{\mathrm{s}}') - g_0^2 \sin^2\theta\left(\frac{1}{g_{\mathrm{c}}'} + \frac{1}{g_{\mathrm{s}}'}\right). \tag{B8b}$$

Since the conductance is similar to the tunnel barrier case (upon replacing the exponent $\alpha_{\mathrm{bulk}}, \alpha_{\mathrm{end}} \to \alpha_{\mathrm{imp}}$), the power-law conductance can mimic the scaling behavior observed in our experiment. We therefore take $\alpha \to \alpha_{\mathrm{imp}}$ in Eq. (2) and treat it as an interpolation formula for the current-voltage curve of a TLL in the presence of weak impurities. In this case, V is the voltage difference across the entire wire, so $\gamma = 1$ regardless of the number of impurities. Equation (B8b) allows us to define the effective interaction parameter for the weak-impurity case,

$$g_{\mathrm{c,eff}}^{\mathrm{imp}} \equiv \cos^2\theta(g_{\mathrm{c}}' + g_{\mathrm{s}}') + g_0^2 \sin^2\theta\left(\frac{1}{g_{\mathrm{c}}'} + \frac{1}{g_{\mathrm{s}}'}\right) - 1. \tag{B9}$$

In the bottom panel of Fig. 8, we plot $g_{\mathrm{c,eff}}^{\mathrm{imp}}$ vs g_{c}. We see that the value of $g_{\mathrm{c,eff}}^{\mathrm{imp}}$ is barely changed, so neither in this case the SOI leads to substantial effects on the extracted value of the interaction parameter.

In summary, for all the types of resistance sources we consider here, the effects of SOI on the extracted value of g_{c} are negligible. Therefore the experimental values of g_{c} can be extracted using equations without including the spin-orbit effects, as given in the main text.

2. Extracting the interaction parameters in various scenarios

In this section, we discuss how the theoretically developed results in the previous section are applied to our experimental data, in order to extract the interaction parameters of our quantum wires. Since SOI leads to negligible changes in the parameter α, in the following we use its zero-SOI form. We express α as a function of g_{c} considering the resistance contributions arising from up to two tunnel barriers and many weak impurities. The former is suggested by the observed value of $1/\gamma \lesssim 2$, and the latter is believed to be present since our wires are relatively long on the scale of the bulk mean free path.

We examine the following scenarios: (A) all barriers are in the bulk and (B) all are around the boundaries of the wire (between the TLL and FL). For both we also add the resistance contributions from weak impurities, and the contact resistance.

In scenario A, weak impurities, both the tunnel barriers in the wire and the contact resistance $R_0 = h/2e^2$ contribute to the total resistance,

$$\begin{aligned} R_{\mathrm{A}}(T,V) &= \frac{1}{G_{\mathrm{bulk}}(T,V)} + \frac{1}{G_{\mathrm{imp}}(T,V)} + R_0 \\ &= \sum_{b=1}^{1/\gamma} R_b\left[\frac{\Delta_a}{\mathrm{Max}(k_BT, \gamma eV)}\right]^{\alpha_{\mathrm{bulk}}} \\ &\quad + R_i\left[\frac{\Delta_a}{\mathrm{Max}(k_BT, eV)}\right]^{\alpha_{\mathrm{imp}}} + R_0. \end{aligned} \tag{B10}$$

Here, $1/\gamma$ is the number of bulk barriers, indexed by b, each with a bare resistance scale R_b. Further, R_i is the bare resistance scale of the disorder potential and Δ_a is the effective bandwidth introduced in the bosonization scheme. Assuming that the two bare resistances are of the same order $O(R_b) = O(R_i)$, the relative magnitude of the barrier and disorder contributions is determined by the exponents α_{bulk} and α_{imp}. Because under experimental conditions Δ_a is much larger than k_BT and eV, the term with the larger exponent dominates (also over the contact resistance). We therefore consider the case where the resistance due to the bulk barriers dominates (that is, when $\alpha_{\mathrm{bulk}} \geqslant \alpha_{\mathrm{imp}}$), which leads to the following condition:

$$\alpha_{\mathrm{bulk}} \gtrsim \alpha_{\mathrm{imp}} \Leftrightarrow g_{\mathrm{c}} \lesssim 1, \tag{B11}$$

where the approximation arises from the assumptions of $O(R_b) = O(R_i)$, $g_{\mathrm{s}} = 1$, and negligible effects from SOI.

Therefore, when the tunnel barriers are in the bulk, the contribution from the barriers dominates over the one from weak impurities for any repulsive interaction. Consequently, in scenario A, the impurity-induced resistance is negligible, and we obtain the conductance

$$\begin{aligned} G_{\mathrm{A}}(T,V) &= \frac{1}{R_{\mathrm{A}}(T,V)} \\ &\approx G_{\mathrm{bulk}}(T,V) \propto \mathrm{Max}(k_BT, \gamma eV)^{\alpha_{\mathrm{bulk}}}, \end{aligned} \tag{B12}$$

resulting in the universal scaling formula in Eq. (2), with $\alpha = \alpha_{\mathrm{bulk}}$. In the main text, we therefore use Eq. (5) to extract the g_{c} value.

We now turn to scenario B, in which there are many weak impurities coexisting with tunnel barrier(s) around the wire end(s). We get

$$\begin{aligned} R_{\mathrm{B}}(T,V) &= \frac{1}{G_{\mathrm{end}}(T,V)} + \frac{1}{G_{\mathrm{imp}}(T,V)} + R_0 \\ &= \sum_{b=1}^{1/\gamma} R_b\left[\frac{\Delta_a}{\mathrm{Max}(k_BT, \gamma eV)}\right]^{\alpha_{\mathrm{end}}} \\ &\quad + R_i\left[\frac{\Delta_a}{\mathrm{Max}(k_BT, eV)}\right]^{\alpha_{\mathrm{imp}}} + R_0. \end{aligned} \tag{B13}$$

The condition for the dominant contribution from the barriers follows as

$$\alpha_{\mathrm{end}} \gtrsim \alpha_{\mathrm{imp}} \Leftrightarrow g_{\mathrm{c}} \lesssim \frac{1}{2}. \tag{B14}$$

As a result, there is a transition of the dominant resistance source when varying g_{c} through the top gate voltage. The

dominant source changes from the tunnel barriers in the strong-interaction regime ($g_c \leqslant 1/2$) to the weak impurities in the weak-interaction regime ($g_c \geqslant 1/2$). We get

$$G_B(T,V) \propto \begin{cases} \mathrm{Max}(\mathrm{k_B T}, \gamma \mathrm{eV})^{\alpha_{\mathrm{end}}}, & \text{for } g_c \leqslant 1/2, \\ \mathrm{Max}(k_B T, eV)^{\alpha_{\mathrm{imp}}}, & \text{for } g_c \geqslant 1/2, \end{cases} \quad \text{(B15)}$$

with the exponents α_{end} and α_{imp} given in Eqs. (B7) and (B8b), respectively.

Interestingly our calculation also suggests that the parameter α should be larger than 0.5 for $g_c \leqslant 1/2$, and smaller than 0.5 for $g_c \geqslant 1/2$. Therefore, in scenario B, we are able to identify the transition of the dominant resistance source based on the observed α values. When $\alpha \geqslant 0.5$, the resistance is due to the boundary tunnel barrier(s) in the regime $g_c \leqslant 1/2$, and therefore $\gamma \simeq 0.5$ suggests two barriers. On the other hand, when $\alpha \leqslant 0.5$, the resistance arises from the impurities, and γ becomes unity.

Consequently the interpolation formula for scenario B is given by Eq. (2), with the parameters

$$(\alpha, \gamma) = \begin{cases} (\alpha_{\mathrm{end}}, \gamma), & \text{for } \alpha \geqslant 0.5 \text{ (barriers);} \\ (\alpha_{\mathrm{imp}}, 1), & \text{for } \alpha \leqslant 0.5 \text{ (impurities).} \end{cases} \quad \text{(B16)}$$

In the main text we use Eq. (8) to extract the value for g_c from the observed α values. Remarkably, upon increasing V_g, we observe that α decreases below 0.5 *around the same* V_g *value* at which γ changes from $\simeq 0.5$ toward unity. This observation is consistent with scenario B, which provides an explanation for the change in γ.

Finally we comment on a third scenario. Namely, one may consider having both types of barriers, bulk and boundary. However, in contrast to our experimental observations this scenario would give conductance with different power laws in the high-bias and high-temperature limits, as discussed in Ref. [50]. We therefore conclude that this scenario is not relevant to our observations.

In summary, the combined experimental and theoretical results for the considered scenarios indicate that our extracted value of $g_c = 0.16$–0.28 is not an artifact of the strong SOI in the InAs wires. This conclusion holds regardless of whether scenario A or B is realized.

3. Summary of the power-law conductance in various TLLs

In this section, we give a summary of the parameter α for various TLL systems. This allows us to compare the interaction parameters in various one-dimensional systems listed in Table I in the main text. Specifically, the summary includes a spinless TLL, a spinful TLL (without SOI), and a spinful TLL with valley degrees of freedom (that is, a carbon nanotube).

In Table II, we list the exponent $\alpha_{\mathrm{bulk}}/\alpha_{\mathrm{end}}/\alpha_{\mathrm{imp}}$ for various TLLs subject to tunnel barriers and many weak impurities. We remark that the exponents $\alpha_{\mathrm{bulk}}/\alpha_{\mathrm{end}}$ are the same for single and multiple tunnel barriers in the wire. The first column gives the system type. The second column corresponds to the scenario in which the tunnel barriers (isolated, strong impurities) are located in the bulk of a wire (that is, TLL-TLL junctions), with the references given in the third column. The fourth column corresponds to the tunnel barriers located around the boundaries of the wire (that is, TLL-FL junctions), with the corresponding references in the fifth column. The sixth column gives the exponent α_{imp} for various TLLs subject to many weak impurities, with the references in the seventh column. In contrast to $\alpha_{\mathrm{bulk}}/\alpha_{\mathrm{end}}$ in the tunneling regime, the value of α_{imp} is bounded. In the table, we give the allowed ranges, assuming that the electron-electron interactions only act on one sector. For example, for a spinful TLL, we assume that the spin sector is noninteracting, $g_s = 1$. For repulsive interactions, the interaction parameter of the charge sector is in the range $g_c \in [0, 1]$, leading to a bound $\alpha_{\mathrm{imp}} \in [0, 1]$.

TABLE II. Exponent α of the power-law conductance in various TLLs subject to tunnel barriers and many weak impurities (treated as weak potential disorder). The first column lists the system types. The second (fourth) column corresponds to the exponent α_{bulk} (α_{end}) for a TLL-TLL (TLL-FL) junction. The sixth column lists the exponents α_{imp} corresponding to many weak impurities. The references corresponding to the entries are given in the third, fifth, and seventh columns. The eighth column lists the allowed ranges for α_{imp}, assuming that only one of the sectors is interacting (with the interaction parameters of the other sectors set to unity). In the entries, the notation g denotes the interaction parameter in a spinless TLL, while the notation $g_{c/s}$ denotes the interaction parameter of the charge/spin sectors, respectively, in a spinful TLL (no SOI). For a spinful TLL with the valley degrees of freedom (for example, a carbon nanotube), the notation $g_{\nu P}$ denotes the sectors of the charge/spin degrees of freedom (with $\nu \in \{c, s\}$, respectively), and the symmetric/antisymmetric combination of the valleys (with $P \in \{S, A\}$, respectively). The quantities after the approximation symbols ($\approx$) indicate the values of the exponents with g_s, g_{cA}, g_{sS}, g_{sA} set to unity. Additional references are given in the footnotes below the table.

TLL type	Bulk barrier α_{bulk}	Refs.	Boundary barrier α_{end}	Refs.	Weak impurities α_{imp}	Refs.	Allowed range[a] for α_{imp}
spinless	$2g^{-1} - 2$	[60,69]	$g^{-1} - 1$	[60]	$2 - 2g$	[59,60,70]	[0, 2]
spinful	$g_c^{-1} + g_s^{-1} - 2$	[59]	$\frac{1}{2}(g_c^{-1} + g_s^{-1}) - 1$	[71]	$2 - g_c - g_s$	[59,70][b]	[0, 1]
	$\approx g_c^{-1} - 1$		$\approx \frac{1}{2}(g_c^{-1} - 1)$		$\approx 1 - g_c$		
spinful with two valleys[d]	$\frac{1}{2}g_{\mathrm{sum}}^{\mathrm{inv}} - 2$	[73][c]	$\frac{1}{4}g_{\mathrm{sum}}^{\mathrm{inv}} - 1$	[39,49,75]	$2 - \frac{1}{2}g_{\mathrm{sum}}$	[75,76][c]	[0, 1/2]
	$\approx \frac{1}{2}(g_{cS}^{-1} - 1)$		$\approx \frac{1}{4}(g_{cS}^{-1} - 1)$		$\approx \frac{1}{2}(1 - g_{cS})$		

[a]Assuming that $g,\ g_c,\ g_{cS} \in [0, 1]$.
[b]See also the calculation in the presence of the multibands or multiple channels [72].
[c]See also the calculation for multiwall nanotubes or ropes of single-wall nanotubes [74].
[d]For this entry, we define $g_{\mathrm{sum}} = g_{cS} + g_{cA} + g_{sS} + g_{sA}$ and $g_{\mathrm{sum}}^{\mathrm{inv}} = g_{cS}^{-1} + g_{cA}^{-1} + g_{sS}^{-1} + g_{sA}^{-1}$.

[1] S.-i. Tomonaga, Prog. Theor. Phys. **5**, 544 (1950).
[2] J. M. Luttinger, J. Math. Phys. **4**, 1154 (1963).
[3] K. A. Matveev, Phys. Rev. B **70**, 245319 (2004).
[4] A. Furusaki and N. Nagaosa, Phys. Rev. B **47**, 4631 (1993).
[5] S. Datta and B. Das, Appl. Phys. Lett. **56**, 665 (1990).
[6] J. Fabian, A. Matos-Abiague, C. Ertler, P. Stano, and I. Žutić, Acta Physica Slovaca **57**, 565 (2007).
[7] R. M. Lutchyn, J. D. Sau, and S. Das Sarma, Phys. Rev. Lett. **105**, 077001 (2010).
[8] Y. Oreg, G. Refael, and F. von Oppen, Phys. Rev. Lett. **105**, 177002 (2010).
[9] J. Klinovaja, P. Stano, and D. Loss, Phys. Rev. Lett. **109**, 236801 (2012).
[10] J. Alicea, Phys. Rev. B **81**, 125318 (2010).
[11] J. Klinovaja and D. Loss, Phys. Rev. B **90**, 045118 (2014).
[12] M. Thakurathi, P. Simon, I. Mandal, J. Klinovaja, and D. Loss, Phys. Rev. B **97**, 045415 (2018).
[13] P. Fendley, J. Stat. Mech.: Theory Exp. (2012) P11020.
[14] A. Hutter and D. Loss, Phys. Rev. B **93**, 125105 (2016).
[15] S. Baba, C. Jünger, S. Matsuo, A. Baumgartner, Y. Sato, H. Kamata, K. Li, S. Jeppesen, L. Samuelson, H. Q. Xu, C. Schönenberger, and S. Tarucha, New J. Phys. **20**, 063021 (2018).
[16] K. Ueda, S. Matsuo, H. Kamata, S. Baba, Y. Sato, Y. Takeshige, K. Li, S. Jeppesen, L. Samuelson, H. Xu, and S. Tarucha, arXiv:1810.04832.
[17] W. Chang, S. M. Albrecht, T. S. Jespersen, F. Kuemmeth, P. Krogstrup, J. Nygård, and C. M. Marcus, Nat. Nanotechnol. **10**, 232 (2015).
[18] P. Krogstrup, N. L. B. Ziino, W. Chang, S. M. Albrecht, M. H. Madsen, E. Johnson, J. Nygård, C. M. Marcus, and T. S. Jespersen, Nat. Mater. **14**, 400 (2015).
[19] M. Kjaergaard, F. Nichele, H. J. Suominen, M. P. Nowak, M. Wimmer, A. R. Akhmerov, J. A. Folk, K. Flensberg, J. Shabani, C. J. Palmstrøm, and C. M. Marcus, Nat. Commun. **7**, 12841 (2016).
[20] A. V. Moroz, K. V. Samokhin, and C. H. W. Barnes, Phys. Rev. Lett. **84**, 4164 (2000).
[21] A. V. Moroz, K. V. Samokhin, and C. H. W. Barnes, Phys. Rev. B **62**, 16900 (2000).
[22] W. Häusler, Phys. Rev. B **63**, 121310(R) (2001).
[23] A. D. Martino and R. Egger, Europhys. Lett. **56**, 570 (2001).
[24] M. Governale and U. Zülicke, Phys. Rev. B **66**, 073311 (2002).
[25] A. Iucci, Phys. Rev. B **68**, 075107 (2003).
[26] M. Governale and U. Zülicke, Solid State Commun. **131**, 581 (2004).
[27] W. Häusler, Phys. Rev. B **70**, 115313 (2004).
[28] J. Sun, S. Gangadharaiah, and O. A. Starykh, Phys. Rev. Lett. **98**, 126408 (2007).
[29] A. Schulz, A. De Martino, P. Ingenhoven, and R. Egger, Phys. Rev. B **79**, 205432 (2009).
[30] N. Kainaris and S. T. Carr, Phys. Rev. B **92**, 035139 (2015).
[31] C. J. Pedder, T. Meng, R. P. Tiwari, and T. L. Schmidt, Phys. Rev. B **94**, 245414 (2016).
[32] C. J. Pedder, T. Meng, R. P. Tiwari, and T. L. Schmidt, Phys. Rev. B **96**, 165429 (2017).
[33] R. Hevroni, V. Shelukhin, M. Karpovski, M. Goldstein, E. Sela, H. Shtrikman, and A. Palevski, Phys. Rev. B **93**, 035305 (2016).
[34] S. Heedt, N. Traverso Ziani, F. Crépin, W. Prost, S. Trellenkamp, J. Schubert, D. Grützmacher, B. Trauzettel, and T. Schäpers, Nat. Phys. **13**, 563 (2017).
[35] S. Tarucha, T. Honda, and T. Saku, Solid State Commun. **94**, 413 (1995).
[36] T. Asayama, Y. Tokura, S. Miyashita, M. Stopa, and S. Tarucha, Physica E **12**, 186 (2002).
[37] E. Levy, A. Tsukernik, M. Karpovski, A. Palevski, B. Dwir, E. Pelucchi, A. Rudra, E. Kapon, and Y. Oreg, Phys. Rev. Lett. **97**, 196802 (2006).
[38] E. Levy, I. Sternfeld, M. Eshkol, M. Karpovski, B. Dwir, A. Rudra, E. Kapon, Y. Oreg, and A. Palevski, Phys. Rev. B **85**, 045315 (2012).
[39] M. Bockrath, D. H. Cobden, J. Lu, A. G. Rinzler, R. E. Smalley, L. Balents, and P. L. McEuen, Nature (London) **397**, 598 (1999).
[40] H. W. C. Postma, M. de Jonge, Z. Yao, and C. Dekker, Phys. Rev. B **62**, R10653 (2000).
[41] E. Graugnard, P. J. de Pablo, B. Walsh, A. W. Ghosh, S. Datta, and R. Reifenberger, Phys. Rev. B **64**, 125407 (2001).
[42] A. Bachtold, M. de Jonge, K. Grove-Rasmussen, P. L. McEuen, M. Buitelaar, and C. Schönenberger, Phys. Rev. Lett. **87**, 166801 (2001).
[43] K. Liu, P. Avouris, R. Martel, and W. K. Hsu, Phys. Rev. B **63**, 161404(R) (2001).
[44] J. Lee, S. Eggert, H. Kim, S.-J. Kahng, H. Shinohara, and Y. Kuk, Phys. Rev. Lett. **93**, 166403 (2004).
[45] J. Luo, H. Munekata, F. F. Fang, and P. J. Stiles, Phys. Rev. B **41**, 7685 (1990).
[46] C. Fasth, A. Fuhrer, L. Samuelson, V. N. Golovach, and D. Loss, Phys. Rev. Lett. **98**, 266801 (2007).
[47] Y. Kanai, R. Deacon, S. Takahashi, A. Oiwa, K. Yoshida, K. Shibata, K. Hirakawa, Y. Tokura, and S. Tarucha, Nat. Nanotechnol. **6**, 511 (2011).
[48] S. Matsuo, H. Kamata, S. Baba, R. S. Deacon, J. Shabani, C. J. Palmstrøm, and S. Tarucha, Phys. Rev. B **96**, 201404(R) (2017).
[49] L. Balents, arXiv:cond-mat/9906032.
[50] L. Venkataraman, Y. S. Hong, and P. Kim, Phys. Rev. Lett. **96**, 076601 (2006).
[51] C.-H. Hsu, P. Stano, Y. Sato, S. Matsuo, S. Tarucha, and D. Loss (unpublished).
[52] A. M. Chang, L. N. Pfeiffer, and K. W. West, Phys. Rev. Lett. **77**, 2538 (1996).
[53] E. Slot, M. A. Holst, H. S. J. van der Zant, and S. V. Zaitsev-Zotov, Phys. Rev. Lett. **93**, 176602 (2004).
[54] A. N. Aleshin, H. J. Lee, Y. W. Park, and K. Akagi, Phys. Rev. Lett. **93**, 196601 (2004).
[55] D. Lucot, F. Jabeen, J.-C. Harmand, G. Patriarche, R. Giraud, G. Faini, and D. Mailly, Appl. Phys. Lett. **98**, 142114 (2011).
[56] T. Li, P. Wang, H. Fu, L. Du, K. A. Schreiber, X. Mu, X. Liu, G. Sullivan, G. A. Csáthy, X. Lin, and R.-R. Du, Phys. Rev. Lett. **115**, 136804 (2015).
[57] A. Anthore, Z. Iftikhar, E. Boulat, F. D. Parmentier, A. Cavanna, A. Ouerghi, U. Gennser, and F. Pierre, Phys. Rev. X **8**, 031075 (2018).
[58] A. V. Moroz and C. H. W. Barnes, Phys. Rev. B **60**, 14272 (1999).
[59] C. L. Kane and M. P. A. Fisher, Phys. Rev. B **46**, 15233 (1992).

[60] T. Giamarchi, *Quantum Physics in One Dimension* (Oxford University Press, New York, 2003).
[61] J. Maciejko, C. Liu, Y. Oreg, X.-L. Qi, C. Wu, and S.-C. Zhang, Phys. Rev. Lett. **102**, 256803 (2009).
[62] M. Levinshtein, S. Rumyantsev, and M. Shur, *Handbook Series on Semiconductor Parameters* (World Scientific, Singapore, 1996), Vol. 1.
[63] M. Rother, W. Wegscheider, R. Deutschmann, M. Bichler, and G. Abstreiter, Physica E **6**, 551 (2000).
[64] O. M. Auslaender, A. Yacoby, R. de Picciotto, K. W. Baldwin, L. N. Pfeiffer, and K. W. West, Phys. Rev. Lett. **84**, 1764 (2000).
[65] S. Li and Q. Zhang, RSC Adv. **5**, 28980 (2015).
[66] M. A. Littlejohn, K. W. Kim, and H. Tian, *Properites Lattice-Matched Strained Indium Gall. Arsenide* (INSPEC, London, 1993), pp. 107–116.
[67] B. Braunecker, G. I. Japaridze, J. Klinovaja, and D. Loss, Phys. Rev. B **82**, 045127 (2010).
[68] T. Meng, J. Klinovaja, and D. Loss, Phys. Rev. B **89**, 205133 (2014).
[69] C. L. Kane and M. P. A. Fisher, Phys. Rev. Lett. **68**, 1220 (1992).
[70] D. L. Maslov, Phys. Rev. B **52**, R14368 (1995).
[71] K. A. Matveev and L. I. Glazman, Phys. Rev. Lett. **70**, 990 (1993); L. Vinet and A. Zhedanov, J. Phys. A: Math. Theor. **44**, 085201 (2011).
[72] N. P. Sandler and D. L. Maslov, Phys. Rev. B **55**, 13808 (1997).
[73] Z. Yao, H. W. C. Postma, L. Balents, and C. Dekker, Nature (London) **402**, 273 (1999).
[74] R. Egger, Phys. Rev. Lett. **83**, 5547 (1999).
[75] C. Kane, L. Balents, and M. P. A. Fisher, Phys. Rev. Lett. **79**, 5086 (1997).
[76] R. Egger and A. O. Gogolin, Phys. Rev. Lett. **79**, 5082 (1997).
[77] S. Heedt, W. Prost, J. Schubert, D. Grützmacher, and T. Schäpers, Nano Lett. **16**, 3116 (2016).